IEEE Access
Multidisciplinary ⋮ Rapid Review ⋮ Open Access Journal

Received March 15, 2021, accepted March 18, 2021, date of publication March 23, 2021, date of current version March 30, 2021.

Digital Object Identifier 10.1109/ACCESS.2021.3068245

Fast and Comprehensive Online Parameter Identification of Switched Reluctance Machines

AHMED M. A. OTEAFY, (Senior Member, IEEE)
Joint Smart Grids and Electric Vehicles Research and Development Center (JSEC), Alfaisal University, Riyadh 11533, Saudi Arabia
e-mail: aoteafy@alfaisal.edu

This work was supported in part by New Energy Transfer Company, and in part by the Office of Research, Innovation and Commercialization, Alfaisal University.

ABSTRACT The switched reluctance machine has been an attractive candidate for many applications owing to its simple design and low construction costs, without the use of permanent magnets. However, the double saliency of its stator and rotor poles results in noise-causing torque ripples. And although advanced torque ripple minimization control techniques exist, they rely on modeling the machine, which in turn requires specialized offline experimental setups or online (during operation) parameter identification techniques. To date, existing online techniques are iterative without proof of convergence, do not provide all model parameters, and/or rely on *a priori* information that can change after the machine is commissioned. In this work, an online parameter identification method is developed with a new empirical model of its flux linkage and electromagnetic torque, to provide a complete nonlinear model of the machine. With two seconds of data collected online, all electrical and mechanical parameters are identified using a non-iterative algorithm, and so it does not pose a risk of divergence. Therefore, parameter identification can be reliably and frequently carried out at different operating conditions as the machine ages for diagnostics. Also, the resulting model is designed to be used by advanced torque ripple minimization control techniques. The implementation procedure is detailed along with simulation results to demonstrate its efficacy.

INDEX TERMS Switched reluctance machine, online parameter identification, nonlinear model, noniterative techniques.

NOMENCLATURE

SRM Variables

v_s, i_s	Stator voltage and current.
θ, ω	Mechanical rotor angular position and velocity.
τ_e	Induced electromagnetic torque.
τ_L	Load torque.
ψ_s	Stator flux linkage.

Subscripts

s	Stator phase, $s \in \{a, b, c\}$.
d, q	Direct and quadrature axes.

Flux Linkage and Torque Empirical Model

$\psi_d(i_s)$	Direct-axis flux linkage function.
$\psi_q(i_s)$	Quadrature-axis flux linkage function.
l_1, l_2, l_3	Parameters of $\psi_d(i_s)$.
L_q	Quadrature-axis inductance.
$f(\theta)$	Flux linkage transition function.
$f'(\theta)$	$\triangleq \partial f(\theta)/\partial\theta$. Partial derivative of $f(\theta)$.
$g(i_s)$	Current-scaling function of τ_e.

SRM Parameters

R_s	Resistance per stator phase.
J_s, B_f	Combined coefficients of the moment of inertia and viscous friction of the SRM and load.
N_s, N_r	Number of stator and rotor poles.
m	Number of stator phases.
α_s	Phase shift angle between stator phases.
ρ	Torque production (cycle) capability angle.
β	Torque zone angle, $= \rho/2$.

Identification Model

y, W	Regressor vector and matrix.
K	Vector of unknown parameters.
N	Total number of sampled data points.
n	Index of sampled data points.

The associate editor coordinating the review of this manuscript and approving it for publication was Yanbo Chen.

ν	Indicator function for data within a valid range.
$u_s(.)$	Unit step function.
EI	Identification model error index.
$\bar{e}_x$	Normalized relative error of a variable $x(t)$.

I. INTRODUCTION

Modeling and parameter identification of electric machines (motors or generators) is an important first step towards their reliable analysis and control. Towards that end, parameter identification methods have been developed for their often nonlinear models, with objectives as varied as performing stability analyses and enhancing controller performance. These methods have been developed for the induction motor [1], [2], the salient-pole synchronous generator [3], and the divided-winding synchronous generator [4] to name a few. For some machines, effective control techniques, such as the PID method, exist that do not rely on an accurate model [5]. However, for other applications such as the switched reluctance machine (SRM), model-based closed-loop control enhances their performance.

The SRM is characterized by its ability to operate at synchronous speed without the use of field windings or permanent magnets. As such, it has a wide range of applications from vacuum cleaners and lathe machines to (potentially) electric vehicles; e.g., see the comparative study on electric vehicle motors by Ramamurthy *et al.* [6]. Its structure, however, has a double saliency, both in its rotor and stator poles, which results in torque ripples and vibrations when basic commutation control schemes are used. Instead, closed-loop control aiming at torque ripple minimization is used, which requires knowledge of its model including the nonlinear flux linkage curves, and the induced electromagnetic torque in relation to the phase current and rotor position, i.e., the τ-i-θ characteristics. In many cases these models are obtained from experimental data to support such control techniques. For example, a feedback linearization technique developed by Ilic-Spong *et al.* [7] achieves robust position tracking control of the SRM using a nonlinear model. The model parameters were determined offline from experimental flux linkage data (to best fit them) enabling their control method. Also, adaptive fuzzy control was used by Mir *et al.* [8] and sliding mode control was used by Inanc and Ozbulur [9] for torque ripple minimization. The latter, for example, required model parameters, namely, the rotor moment of inertia and slope of inductance with respect to rotor angle variations. Several other SRM control methods were developed including the use of torque sharing functions in [10], [11], a hybrid PID torque sharing with τ-i-θ characteristics in [12], and the use of model predictive control and a Kalman filter with recursive least squares to estimate the inductances in [13].

Flux linkage curves can therefore be computed experimentally as in [14], [15], using finite element analysis methods (FEM) as in [16], [17], or as empirical analytical functions that approximate these curves at various rotor positions and current levels, see for example Le-Huy and Brunelle [18]. Using these curves the τ-i-θ characteristics can then be determined for use in the aforementioned control methods. Ultimately, the model obtained for the τ-i-θ characteristics is either a look up table or an empirical analytical model that best fits the data. The former method can be more accurate in implementation (provided enough data points are recorded) but requires a large memory on the controller. Therefore, empirical analytical models are preferred for microcontroller operated motor drives due to their lower computational complexity in memory and time. Miller and McGilp [19], for example, capture the flux nonlinear curves transitioning between the unaligned and aligned rotor positions using parameterized piecewise functions and correction factors. Their parameters and correction factors are calculated from a limited set of points obtained from FEM. Their model was later improved [20], with the introduction of smooth transitions in their normalized flux *gage* curves. Also, Vujicic and Vukosavic [21] propose a set of three parameterized piecewise functions to characterize the flux linkage curve with the parameters calculated from the SRM geometry, magnetic material and points on the experimental curves.

Parameter identification for a given model could be further categorized as offline or online depending on whether the SRM is disconnected from its load with a dedicated experimental excitation setup or connected to its operational load, respectively. Typically, offline methods aim to obtain detailed flux linkage curves and are performed prior to commissioning the SRM. The challenges of experimentally obtaining these curves offline are discussed by Sharma *et al.* [14] with a recommendation for example to use a fixed DC source as excitation to reduce measurement noise and simplify filtering requirements. In their offline method, the test had to be repeated in standstill at different rotor angles. Data collection periods also vary depending on whether the test requires capturing steady state signals or transient signals, with the former requiring significantly longer times. By adding a search coil on the stator to measure the EMF, Ferrero and Raciti [22] showed that AC excitation can be used with the SRM in standstill or a DC excitation with the rotor moved using another motor during data acquisition to obtain the flux linkage curves. Alternatively, FEM can be used in the design phase and later verified from experimental data, see for example by Ursu *et al.* [17].

Online methods have also been developed to directly obtain the parameters of an empirical model of the SRM. They are non-intrusive to the operation of the SRM and can be conducted periodically, e.g., at different operating conditions and as the machine ages. Mir *et al.* [23] developed an iterative (recursive) online method for torque estimation to aid their fuzzy controller [8]. A single parameterized function for the flux curve was used with a few parameters to be measured offline such as the stator resistance, and five parameters to be recursively computed and improved online. This function was later reduced to four parameters [24] to improve the chances of convergence. Also, online identification methods for the linear SRM were developed by Pan *et al.* [25] for

position control, and by Missouri *et al.* [26] to aid their fuzzy system based controller. However, iterative methods require a proof of convergence as they may diverge during their implementation. A more recent iterative method developed by Aguado-Rojas *et al.* [27] identifies all electrical and mechanical SRM model parameters online. Moreover, their work outlines a proof of convergence of their iterative method that can be tested by the algorithm during its execution. However, their model assumes linear magnetics which limits its applicability to very low current levels that are well below the rated current of a typical SRM.

In this work, an online parameter identification method is developed for the SRM, with the following contributions:

1) A new empirical nonlinear model of the SRM flux linkage and torque is introduced.
2) All electrical and mechanical parameters of the model are identified online.
3) Offline tests and *a priori* knowledge of the SRM are not needed.
4) Its algorithm is non-iterative and hence can reliably work without the need to prove its convergence or risk divergence.
5) Its procedure is detailed and carried out with two seconds of data, which can run on an SRM embedded system drive.

Therefore, in contrast with existing online methods, it is both comprehensive and reliable. The remainder of the paper is organized as follows: The machine model is given in Section II, and its parameter identification models are derived in Section III. The implementation in simulation and its results are detailed in Section IV, with the impact of disturbance considered and an alternative online method included for comparison. Concluding remarks are drawn in Section V.

II. MODELING THE SRM

The dynamic model of the SRM using the motor (load) convention represents the electrical and mechanical dynamics as follows, see Le-Huy and Brunelle [18] and Gieras [28]

$$v_s = \frac{d\psi_s}{dt} + R_s i_s, \tag{1}$$

$$\tau_e(i,\theta) = J\frac{d\omega}{dt} + B_f\omega + \tau_L, \tag{2}$$

$$\frac{d\theta}{dt} = \omega. \tag{3}$$

There are m stator phases, with the subscript s denoting any one of these phases, e.g., for a three phase machine $m = 3$ and $s \in \{a, b, c\}$. For the electrical quantities, v_s is the terminal voltage, i_s is the current, ψ_s is the flux linkage, and R_s is the resistance per stator phase. For the mechanical dynamics τ_e is the induced electromagnetic torque, which is a function of both i_s and the rotor position θ. Also, ω is the rotor angular velocity, τ_L is the load torque. J and B_f are the rotor coefficients of the moment of inertia and viscous friction, respectively.

A prominent feature of an SRM is its double saliency, and the number of stator poles N_s and rotor poles N_r are not equal. To operate the SRM, a complete cycle of pulses and torque production is identified as its periodicity, or the torque production capability angle, and is given by $\rho \triangleq 2\pi/N_r$. A related angle is the torque zone [28], which is half of the periodicity, and can be defined as $\beta \triangleq \rho/2 = \pi/N_r$. So, a voltage is applied in each stator phase to generate a current pulse resulting in a magnetic field attracting the rotor poles. The angle over which one phase can influence torque is called the stroke angle $\alpha_s \triangleq 2\pi/(mN_r)$, which is also the phase shift between stator phases.

Therefore, the rotor pole starts from an aligned position with stator phase a at $\theta = 0$ rad and reaches the quadrature point (furthest from this alignment) at $\theta = \beta$. The next rotor pole reaches full alignment with stator phase a at $\theta = 2\beta$.

One SRM configuration that will be adopted in this work without loss of generality is the 6/4 SRM with $N_s = 6$ and $N_r = 4$ as shown in Fig. 1. This has $m = 3$ stator phases, $\beta = \pi/4$ rad and $\alpha_s = \pi/6$ rad. Note that there is no need to define an electrical counterpart to the mechanical angle θ. That is, θ suffices for modeling both mechanical and electrical dynamics of the SRM [7].

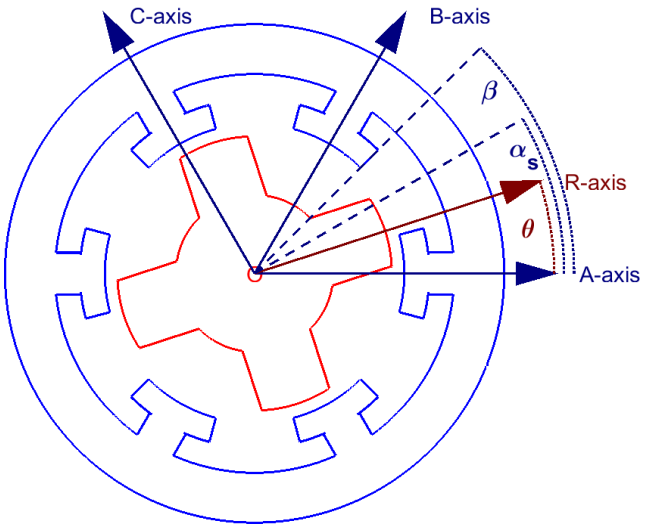

FIGURE 1. A 6/4 SRM with its axes and angles.

A. FLUX LINKAGE CHARACTERISTICS

Assuming no mutual coupling between the phases, ψ_s only depends on its self-inductance. However, the machine is typically operated in the magnetic saturation region, making ψ_s nonlinearly dependent on i_s. Also, the reluctance along the path of the magnetic flux significantly changes as the SRM rotates due to its double saliency, hence, it is both a function of i_s and θ, i.e., $\psi_s(i_s, \theta)$. If v_s, i_s, and R_s are known, ψ_s can be computed *directly* by integrating both sides of (1) and rearranging to get

$$\psi_s(t) = \int_{t'=t_0}^{t'=t} v_s - R_s i_s \, dt', \tag{4}$$

where t_0 is the moment when commutation starts and t' is a dummy integration variable evaluated in the time range $t > t_0$ such that $i_s(t) \neq 0$ and $i_s(t_0) = 0$. Note that $\psi_s(t_0) = 0$, and, in general, ψ_s must be reset to zero whenever $i_s = 0$ because the SRM stator and rotor are constructed using soft ferromagnetic materials, i.e., they do not retain a residual magnetic field. Therefore, the integrator reset is an important step when using this method in a simulation or on a microcontroller to calculate ψ_s.

Alternatively, $\psi_s(i_s, \theta)$ can be obtained using one of two methods:

1) A look up table constructed with the rotor fixed at specific angles in the range $0 \leq \theta \leq 2\beta$. This requires a large memory allocation in the controller.
2) An approximate parameterized empirical model, with the parameters either obtained to best fit experimental data (of method 1) or from an online parameter identification method as discussed in this work.

One such empirical model was proposed by Le-Huy and Brunelle [18] and is the basis of a new empirical model developed in this work. This model is given by

$$\psi_s(i_s, \theta) = \psi_q(i_s) + \big(\psi_d(i_s) - \psi_q(i_s)\big) f(\theta), \tag{5}$$

where $\psi_d(.)$ is the aligned flux linkage, $\psi_q(.)$ is the quadrature flux linkage, and $f(\theta)$ is a function representing the transition along the range $0 \leq \theta \leq 2\beta$. In other words, the flux linkage is maximum when stator phase a and a rotor pole are directly aligned, with $\psi_s = \psi_d$. In quadrature, $\psi_s = \psi_q$, which occurs at $\theta = \beta$. These flux linkages are functions of the phase current as

$$\psi_d(i_s) = l_1 i_s + l_2 i_s e^{-l_3 i_s}, \tag{6}$$
$$\psi_q(i_s) = L_q i_s, \tag{7}$$

where $\psi_q(i_s)$ is parameterized with L_q, but unlike Le-Huy and Brunelle [18], $\psi_d(i_s)$ is parameterized with l_1, l_2, and l_3. These parameters along with R_s will be obtained using online parameter identification.

In addition, the function representing the transition between $\psi_d(.)$ and $\psi_q(.)$ in (5) is given as [18]

$$f(\theta) = \frac{2N_r^3}{\pi^3}\theta^3 - \frac{3N_r^2}{\pi^2}\theta^2 + 1. \tag{8}$$

Recalling that $\beta \triangleq \pi / N_r$, we can rewrite this equation as

$$f(\theta) = \frac{2}{\beta^3}\theta^3 - \frac{3}{\beta^2}\theta^2 + 1. \tag{9}$$

Note that $\psi_d(.)$ and $\psi_q(.)$ are only functions of the current i_s and $f(.)$ is only a function of θ. This analytical function is similar in form to the work by Miller *et al.* [20], but it is simpler as it has fewer parameters to identify. Based on this model from [18], $f(0) = 1, f(\beta) = 0$ and $f(2\beta) = 5$. Therefore, $f(.)$ is only valid for $0 < \theta < \beta$, i.e., between the aligned (direct) and the unaligned (quadrature) positions of phase a. So, a modification is necessary to make $f(.)$ valid for a complete cycle in the range $0 < \theta < 2\beta$, by redefining it as

$$f(\theta) = \left(\frac{2}{\beta^3}\theta^3 - \frac{3}{\beta^2}\theta^2 + 1\right)(1 - u_s(\theta - \beta)) + \left(\frac{2}{\beta^3}(2\beta - \theta)^3 - \frac{3}{\beta^2}(2\beta - \theta)^2 + 1\right) u_s(\theta - \beta), \tag{10}$$

where $u_s(.)$ is the unit step function. It can be simplified to

$$f(\theta) = \frac{1}{\beta^3}\left[\left(2\theta^3 - 3\beta\theta^2 + \beta^3\right) - 4(\theta - \beta)^3 u_s(\theta - \beta)\right]. \tag{11}$$

Therefore, the flux linkage model is comprised of equations (5), (6), (7) and (11).

B. THE INDUCED ELECTROMAGNETIC TORQUE

The electromagnetic torque $\tau_{e,s}$ resulting from i_s in each phase s is computed from the coenergy function W' as

$$\tau_{e,s} = \frac{\partial W'}{\partial \theta}, \tag{12}$$

where $W' = \int_{\iota=0}^{\iota=i_s} \psi(\iota, \theta) d\iota$.

The coenergy is in turn computed from $\psi_s(i_s, \theta)$ either numerically using the tables or analytically from equation (5). Accordingly,

$$\tau_{e,s}(i_s, \theta) = \frac{\partial W'}{\partial \theta} = \int_{\iota=0}^{\iota=i_s} \frac{\partial \psi(\iota, \theta)}{\partial \theta} d\iota. \tag{13}$$

Then,

$$\frac{\partial \psi(i_s, \theta)}{\partial \theta} = \big(\psi_d - \psi_q\big) \frac{\partial f(\theta)}{\partial \theta}, \tag{14}$$

and

$$f'(\theta) \triangleq \frac{\partial f(\theta)}{\partial \theta} = \frac{6(\theta - \beta)}{\beta^3}\left[\theta - 2(\theta - \beta) u_s(\theta - \beta)\right]. \tag{15}$$

Since this is a derivative of a piecewise function, the derivative of each portion is obtained separately. In this case, the first order derivative at $\theta = \beta$ is zero for both functions. Hence, there is no discontinuity and as a result

$$\tau_{e,s}(i_s, \theta) = \int_{\iota=0}^{\iota=i} \big(\big(\psi_d(\iota) - \psi_q(\iota)\big) f'(\theta)\big)\, d\iota = g(i_s) f'(\theta), \tag{16}$$

where,

$$g(i_s) \triangleq \frac{1}{2}(l_1 - L_q) i_s^2 - \frac{l_2}{l_3} i_s e^{-l_3 i_s} + \frac{l_2}{l_3^2}\left(1 - e^{-l_3 i_s}\right) \tag{17}$$

The total induced electromagnetic torque is the sum

$$\begin{aligned}\tau_e(i_a, i_b, i_c, \theta) &= \tau_{e,a} + \tau_{e,b} + \tau_{e,c} \\ &= g(i_a) f'(\theta) + g(i_b) f'(\theta - \alpha_s) \\ &\quad + g(i_c) f'(\theta - 2\alpha_s),\end{aligned} \tag{18}$$

with $\alpha_s = 2\pi/(mN_r) = \pi/6$ rad being the phase shift between the stator phases.

In summary, the SRM model is given by equations (1), (2), and (3), in addition to

$$\begin{aligned}\psi_s(i_s,\theta) &= \psi_q(i_s) + \big(\psi_d(i_s) - \psi_q(i_s)\big) f(\theta) \\ &= L_q i_s + \Big((l_1 - L_q) i_s + l_2 i_s e^{-l_3 i_s}\Big) f(\theta), \quad (19)\\ \tau_e(i_a,i_b,i_c,\theta) &= g(i_a) f'(\theta) + g(i_b) f'(\theta - \alpha_s) \\ &\quad + g(i_c) f'(\theta - 2\alpha_s), \quad (20)\end{aligned}$$

with $f(\theta)$, $f'(\theta)$ and $g(i_s)$ defined in (11), (15) and (17), respectively.

III. ONLINE PARAMETER IDENTIFICATION MODEL

The identification model is derived next, consisting of electrical and mechanical regressor equations. They are solved in sequence to obtain all the SRM parameters. Also, two error metrics are introduced, namely, an error index and a normalized relative error, which are used as qualifying metrics for the results.

A. ELECTRICAL REGRESSOR

For any phase $s \in \{a, b, c\}$, we substitute (19) in (4) and rearrange to get

$$\begin{aligned}\int_{t'=t_0}^{t'=t} v_s dt' = R_s \int_{t'=t_0}^{t'=t} i_s dt' + L_q i_s (1 - f(\theta)) \\ + l_1 i_s f(\theta) + l_2 i_s e^{-l_3 i_s} f(\theta). \quad (21)\end{aligned}$$

During the online operation of the machine, let the current be regulated at two reference values over two time ranges as

$$i_s \approx \begin{cases} I_{ref\,1}, & \forall t \in (t_{1a}, t_{1b}) \\ I_{ref\,2}, & \forall t \in (t_{2a}, t_{2b}) \end{cases}, \quad (22)$$

for which indicator functions can be defined as

$$\nu_1 \triangleq \begin{cases} 1, & \forall t \in (t_{1a}, t_{1b}) \\ 0, & \text{otherwise.} \end{cases}, \nu_2 \triangleq \begin{cases} 1, & \forall t \in (t_{2a}, t_{2b}) \\ 0, & \text{otherwise.} \end{cases}. \quad (23)$$

We can approximate the last term of (21) as $l_2\ i_s e^{-l_3\ i_s} \approx l_2\ I_{ref} e^{-l_3\ I_{ref}}$ over a given time range, either by tightly regulating the phase current or simply by collecting data points only when they satisfy a tolerance bound ΔI_{tol}, i.e., $\left|I_{ref} - i_s\right| < \Delta I_{tol}$. Representing these equations in regressor form we obtain

$$y = W\ K, \quad (24)$$

with,

$$\begin{aligned} y &\triangleq \left[\ \nu_1 \int_{t'=t_0}^{t'=t} v_s dt'\ \ \nu_2 \int_{t'=t_0}^{t'=t} v_s dt'\ \right]^T, \\ W &\triangleq \begin{bmatrix} \nu_1 \int_{t'=t_0}^{t'=t} i_s dt' & \nu_1 (1 - f(\theta))\, i_s & \nu_1 f(\theta) i_s \\ \nu_2 \int_{t'=t_0}^{t'=t} i_s dt' & \nu_2 (1 - f(\theta))\, i_s & \nu_2 f(\theta) i_s \end{bmatrix} \\ &\quad \begin{bmatrix} \nu_1 f(\theta) & 0 \\ 0 & \nu_2 f(\theta) \end{bmatrix}, \\ K &\triangleq \left[\ \kappa_1\ \kappa_2\ \kappa_3\ \kappa_4\ \kappa_5\ \right]^T \\ &\triangleq \left[\ R_s\ L_q\ l_1\ l_2 I_{ref\,1} e^{-l_3 I_{ref\,1}}\ l_2 I_{ref\,2} e^{-l_3 I_{ref\,2}}\ \right]^T, \end{aligned}$$

where K contains the unknown parameters, whereas y and W are known from the measured variables. The variables are sampled at $t = T, 2T, 3T, \ldots, NT$, where T is the sampling period and N is the total number of samples collected. So y and W are computed for each data point $n = 1$ to N. One desires to find K that minimizes the mean squared error defined by

$$E^2(K) \triangleq \sum_{n=1}^{N} \|y(nT) - W(nT)K\|^2. \quad (25)$$

Multiplying out the right-hand side gives

$$E^2(K) = R_y - R_{Wy}^T K - K^T R_{Wy} + K^T R_W K, \quad (26)$$

where, $R_y = \sum_{n=1}^{N} y^T(nT) y(nT)$, $R_W = \sum_{n=1}^{N} W^T(nT) W(nT)$, and $R_{Wy} = \sum_{n=1}^{N} W^T(nT) y(nT)$.

If R_W is invertible, we can minimize $E^2(K)$ by $\partial E^2(K)/\partial K = -2R_{Wy} + 2R_W K = 0$, that is,

$$K = R_W^{-1} R_{Wy}. \quad (27)$$

After computing K, recall that $\kappa_4 = l_2\ I_{ref\,1} e^{-l_3\ I_{ref\,1}}$ and $\kappa_5 = l_2\ I_{ref\,2} e^{-l_3\ I_{ref\,2}}$, so we need to find l_2 and l_3 from these parameters. Further restricting the reference currents so that $I_{ref\,1} = \frac{1}{2} I_{ref\,2}$, facilitates finding l_2 and l_3 as will be shown. $I_{ref\,2}$ can be the rated current of the machine, or an operating point close to it, resulting in a model that represents a wide range of operating points. However, any other two reference currents can be used so long as they represent the linear and saturation regions of operation. To solve for l_1 and l_2 using $(\kappa_4, I_{ref\,1})$ and $(\kappa_5, I_{ref\,2})$, we divide κ_5 by κ_4, and rearrange to get l_3 as

$$l_3 = \frac{\ln(\kappa_4 I_{ref\,2}) - \ln(\kappa_5 I_{ref\,1})}{I_{ref\,2} - I_{ref\,1}}. \quad (28)$$

Substituting back in κ_5, and solving for l_2 we get

$$l_2 = \frac{\kappa_5}{I_{ref\,2}} e^{l_3 I_{ref\,2}}. \quad (29)$$

B. MECHANICAL REGRESSOR

After finding the electrical parameters, the induced electromagnetic torque can be computed using (2), (20), (15) and (17). Additionally, (2) can be integrated to add a second equation forming the mechanical parameter identification model

$$\tau_e(i,\theta) = J\frac{d\omega}{dt} + B_f \omega + \tau_L \quad (30)$$

$$\int_{t'=0}^{t'=t} \tau_e(i,\theta)\, dt' = J\omega + B_f \theta + \tau_L t \quad (31)$$

Rewriting them in regressor form

$$y_M = W_M\ K_M, \quad (32)$$

where,

$$y_M \triangleq \left[\, \tau_e(i,\theta) \;\; \int_{t'=0}^{t'=t} \tau_e(i,\theta)\, dt' \,\right]^T,$$
$$W_M \triangleq \begin{bmatrix} d\omega/dt & \omega & 1 \\ \omega & \theta & t \end{bmatrix},$$
$$K_M \triangleq \left[\, \kappa_6 \;\; \kappa_7 \;\; \kappa_8 \,\right]^T \triangleq \left[\, J \;\; B_f \;\; \tau_L \,\right]^T.$$

K_M contains the unknown mechanical parameters, whereas y_M and W_M are known from the N sampled measurements. Note that J and B_f represent the combined SRM and load coefficients. Also, τ_L is assumed to be constant over the brief period over which the data is collected. One desires to find K_M that minimizes the mean squared error defined by

$$E^2(K_M) \triangleq \sum_{n=1}^{N} \| y_M(nT) - W_M(nT) K_M \|^2 . \tag{33}$$

where, in this case, $R_y = \sum_{n=1}^{N} y_M^T(nT) y_M(nT)$, $R_W = \sum_{n=1}^{N} W_M^T(nT) W_M(nT)$, and $R_{Wy} = \sum_{n=1}^{N} W_M^T(nT) y_M(nT)$. This was shown to yield $K_M = R_W^{-1} R_{Wy}$.

C. AN ERROR INDEX

The squared errors in (26) and (33) can be used to define an Error Index. This determines how well the identified parameter set K^* provides a best fit for the collected data [3], [5], and is defined as,

$$EI \triangleq \sqrt{E^2(K^*)/E^2(0)} = \sqrt{\left(R_y - 2R_{wy}^T K^* + K^{*T} R_W K^* \right)/R_y} \leq 1, \tag{34}$$

where, the squared error at K^* is compared to the squared error at the zero vector, i.e., $K = \mathbf{0}$. EI should be less than one; otherwise, K^* is as good as any arbitrary set K.

D. A NORMALIZED RELATIVE ERROR

One main objective of the parameter identification method is to produce a model that can estimate the stator flux linkage $\psi_s(t)$ and induced torque $\tau_e(t)$ state variables. Therefore, a useful metric for determining the efficacy of the proposed method is to calculate the relative error between the actual (e.g., from simulation data) and the estimated state variables. This can be defined similar to the state estimation methods in the work by Chen *et al.* [29]–[31] as

$$\bar{e}_x \triangleq \frac{1}{N} \sum_{n=1}^{N} \left| \frac{x_{act}(nT) - x_{est}(nT)}{x_{act}(nT)} \right|, \tag{35}$$

where, x is the state variable of interest (e.g., ψ_s), x_{act} is the measured (or simulated) variable, and x_{est} is its estimated counterpart. Note that in practice, the sampled data must be in a range where $x_{act}(nT)$ is not zero, in which case, N is replaced by the number of samples in this valid range.

IV. IMPLEMENTATION AND RESULTS

The application of the proposed parameter identification method is demonstrated in simulation with the implementation procedure listed in detail. A model of the SRM is constructed in Simulink along with: a mechanical load, a hysteresis current controller, and a data acquisition block, see Fig. 2. Moreover, a three-leg asymmetric bridge converter is used to drive the SRM, which is a standard converter for SRM drives [28].

The model represents an SRM with $N_s = 6$ stator poles, $N_r = 4$ rotor poles, that is rated for an output power of 8 hp at a rotor speed of 860 rpm, and is driven by a converter with a DC bus voltage of 240 V and a rated line current of 180 A. Its parameters include $R_s = 0.3\ \Omega$, $J = 0.05$ kg.m^2, and $B_{f,SRM} = 0.001$ N.m.s. To model a practical mechanical load, both viscous friction and constant torque loads are applied with $B_{f,L} = 0.4$ N.m.s and $\tau_L = 4$ N.m, respectively. For a conveyor belt application, for example, viscous friction load exists at all contact points along the belt and an incline in the belt along with the mass of the loaded objects will present a constant applied torque. If the loaded objects are traveling upwards along the conveyor belt a load torque results, whereas traveling downwards results in a generating torque. Experimental flux linkage data is used with $\psi_{s,\max} = 0.43$ Wb-t, $I_{s,\max} = 180$ A and, the flux linkage curves $\psi_s(i_s, \theta)$ are shown for different i_s and θ values in Fig. 3.

With the SRM inertia and friction moved outside of the SRM block in Fig. 2, $\tau_{ind}(t)$ can be directly measured. Also, when R_s is known, $\psi_s(t)$ can be computed by integrating the v_s and i_s, which is performed by its block in Fig. 2. Both waveforms are used for comparison with their estimated counterparts $\tau_{ind,est}(t)$ and $\psi_{s,est}(t)$, but they are otherwise not needed by the identification method.

The flux linkage curves can be used to obtain $L_q = \psi(180, 45°)/180 = 0.5556$ mH at the quadrature position. However, the remaining parameters have to be obtained to fit the empirical flux linkage model.

A. PARAMETER IDENTIFICATION PROCEDURE

The procedure is detailed in the following steps:

1) With the SRM online and connected to its load, it is brought up to two operating points using a hysteresis current controller, e.g., $I_{s,ref}$ of 75 A and 150 A for a 1 s interval each, with a switching frequency $f_s = 20$ kHz. The hysteresis band is set to $\pm 5\%$ of $I_{s,ref}$. That is, for each active phase $s \in a, b, c$, the switches are turned on when $i_s < I_{s,ref} \times 0.95$, turned off when $i_s > I_{s,ref} \times 1.05$, and kept unchanged otherwise.
2) The collected data includes v_s, i_s, and θ, where the sampling frequency is the same as the switching frequency. It is also helpful to record the active phase $s \in \{a, b, c\}$ during data collection. This facilitates determining the parameters of each phase and separately modeling any asymmetries in the SRM; potentially identifying an imminent failure in one of the phases.

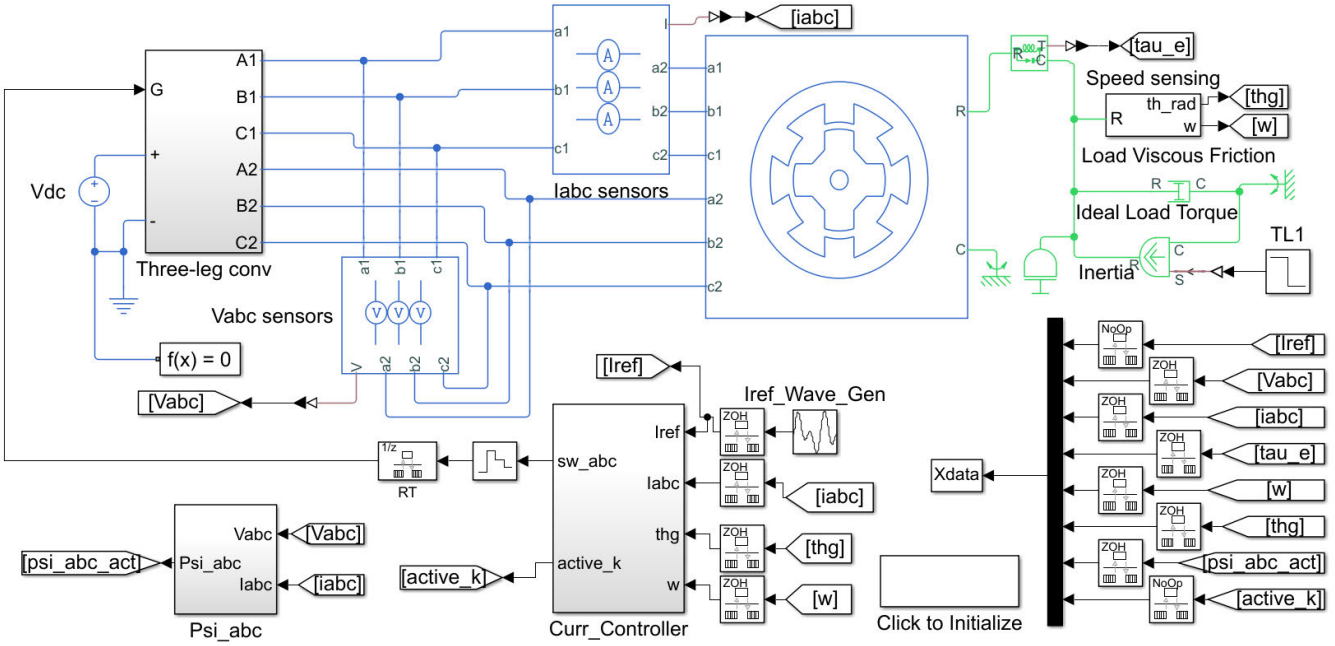

FIGURE 2. SRM Simulink model.

3) Select the data points where the current i_s is within $I_{tol} = \pm 4\%$ around the reference current I_{ref}, i.e., $\left|I_{ref} - i_s\right| / I_{ref} < I_{tol}$.
4) Numerically integrate i_s and v_s, resetting whenever $i_s = 0$. Also, integrate ω to get θ if the latter is not measured.
5) The modulo of the rotor angle θ is taken with periodicity $2\beta = 90°$, and is used to calculate $f(\theta)$ and $f'(\theta)$, in (11) and (15).
6) Set each indicator function ν_1, ν_2 in (15) to 1, whenever its corresponding reference current is active.
7) The sampled data, indexed from $n = 1$ to N, is used to calculate $y(nT)$ and $W(nT)$ in (24) and construct the regressor matrices R_y, R_W & R_{Wy} of (26).
8) With $K = R_W^{-1} R_{Wy}$: $R_s = \kappa_1$, $L_q = \kappa_2$, and $l_1 = \kappa_3$. Also, calculate l_2 and l_3 using (29) and (28), respectively. Its EI is calculated using (34).
9) Use the identified electrical parameters to compute $\tau_e(i_a, i_b, i_c, \theta)$ in (20).
10) Use the same sampled data with a digital low pass filter, e.g., 4^{th} order low pass Butterworth filter set at $f_c = 200$ Hz, and substitute for τ_e, ω, and $d\omega/dt$ to calculate $y_M(nT)$ and $W_M(nT)$ of (32). Note that in Matlab this can be implemented using the `filtfilt` function with the order set to 2, as the function filters the data forward and backward to eliminate phase shifts in the resulting filtered signals.
11) The mechanical regressor matrices R_y, R_W & R_{Wy} of equation (33) are constructed resulting in the vector $K_M = R_W^{-1} R_{Wy}$.
12) Then, the identified mechanical parameters, which combine the SRM and its load, are $J = \kappa_7$ and $B_f = \kappa_8$, and $\tau_L = \kappa_9$, and EI is found using (34).

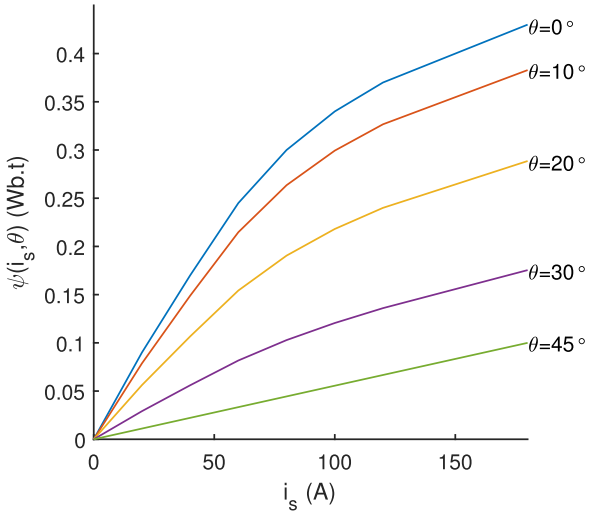

FIGURE 3. SRM model flux linkage data at different angles.

B. SIMULATION RESULTS

The steps of the procedure are implemented on the SRM in Fig. 2. The plots of the measured variables v_a, i_a, and ω are shown in Fig. 4, Fig. 5, and Fig. 6, respectively. The estimated electrical parameters are listed in Table 1 along with the actual (known) values. An error index $EI = 0.0173$ was calculated showing that the parameters resulted in a model that is a good fit for the collected data.

These estimated parameters are used to compute $\psi_{a,est}$ and τ_{est} as shown in Fig. 7 and Fig. 8, respectively. The waveforms show that both estimated waveforms closely follow their measured counterparts. Specifically, the normalized relative errors in these two waveforms are $\bar{e}_\psi = 0.018$ and $\bar{e}_\tau = 0.15$, respectively.

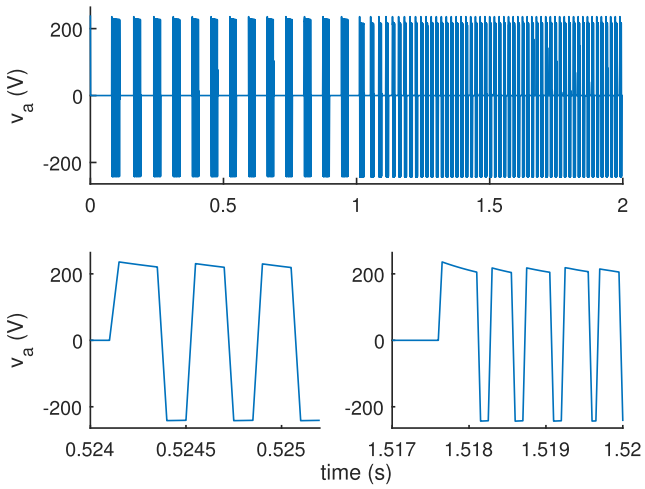

FIGURE 4. Stator voltage v_a vs. time with zoomed subplots.

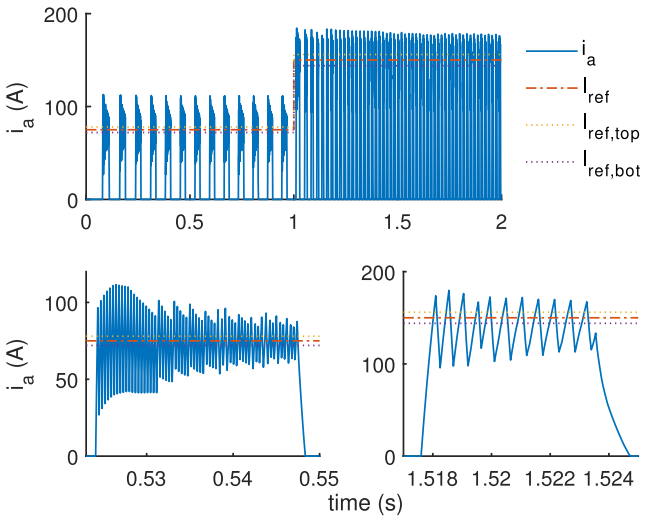

FIGURE 5. Stator current i_a vs. time with I_{ref} and the tolerance bounds with zoomed subplots.

TABLE 1. Electrical parameter identification results.

Parameter	Unit	Estimated Value	Actual Value	Error
R_s	Ω	0.2991	0.3000	0.31%
L_q	mH	0.5594	0.5556	0.69%
l_1	mH	0.8494	–	–
l_2	-	4.001×10^{-3}	–	–
l_3	-	5.563×10^{-3}	–	–

Then, the estimated variables $\psi_{a,est}$ and τ_{est} are used to obtain the mechanical parameters, which are shown in Table 2 along with the actual (known) values. The error index is $EI = 0.066$, which also shows that the parameters are a good fit for the collected data and that the machine is sufficiently excited. In addition, the total execution time of the procedure is 2.45 seconds, with 2.0 seconds for data collection and 0.45 seconds for computations, on a PC with an Intel

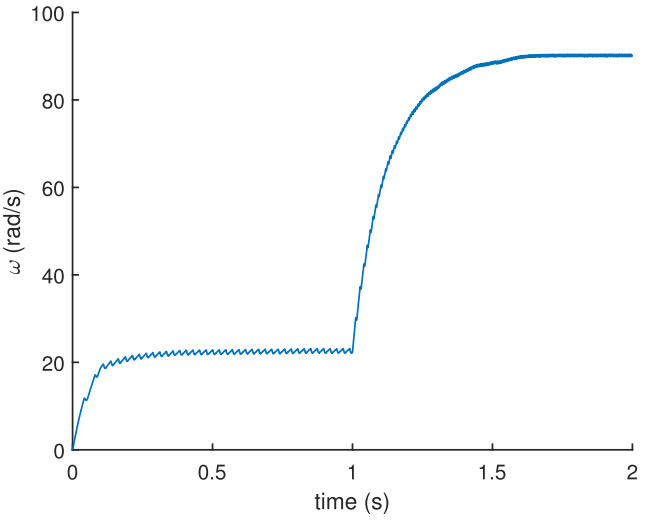

FIGURE 6. Rotor speed ω vs. time.

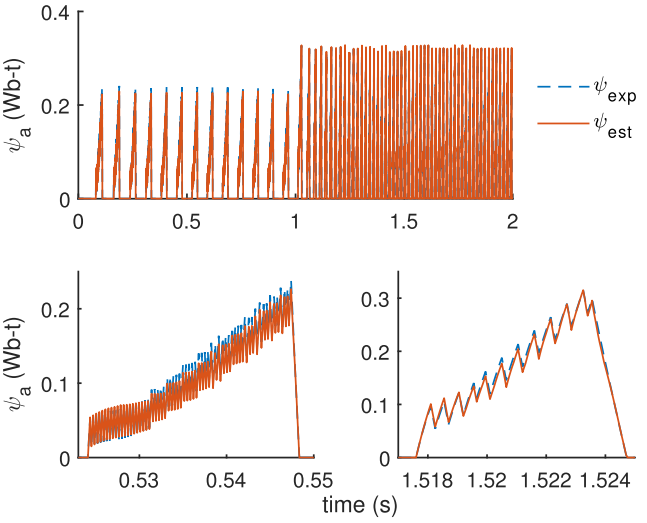

FIGURE 7. Actual ψ_{exp} and estimated ψ_{est} flux linkages vs. time with zoomed subplots.

TABLE 2. Mechanical parameter identification results.

Parameter	Unit	Estimated Value	Actual Value	Error
J	kg.m^2	0.04679	0.05000	6.42%
B_f	N.m.s	0.4021	0.4010	0.28%
τ_L	N.m	3.791	4.000	5.21%

Core i5 CPU operating at 2.40 GHz with an 8 GB RAM. Therefore, the proposed online parameter identification method furnished all electrical and mechanical model parameters of the SRM. Both the plots of the estimated flux and torque obtained from the analytical model proposed in this work are close to those computed from the measured data.

C. IMPACT OF DISTURBANCE

To further validate the proposed online identification method, the impact of disturbance on the measured signal

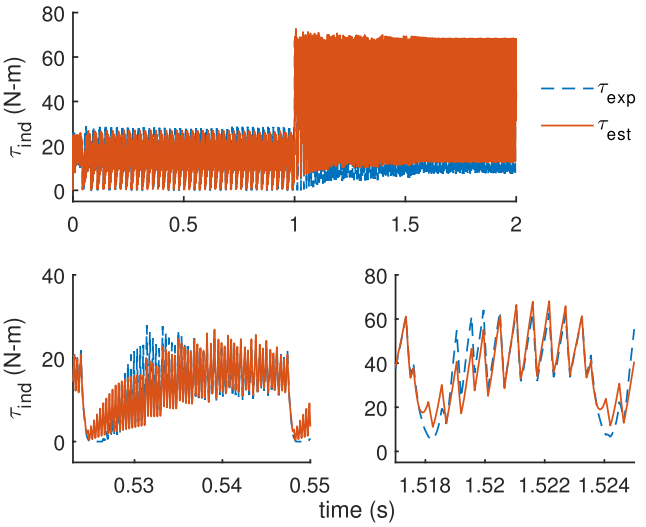

FIGURE 8. Actual τ_{exp} and estimated τ_{est} torques vs. time with zoomed subplots.

is investigated. Specifically, the additive white gaussian noise model function is applied to all the signals that are used by the identification model, namely, v_a, i_a, ω and θ for phase a. Also, v_a and i_a are numerically integrated after the added noise. Then, the same identification algorithm settings are used. Signal to noise ratios of $SNR = 40$ dB, $SNR = 34$ dB and $SNR = 30$ dB are used, with the percentage error in the parameters listed in Table 3. These results show that as the noise levels increase, the electrical parameters are still identified with relatively low errors. However, the performance of the mechanical identification deteriorates with higher noise levels, particularly with regards to τ_L.

TABLE 3. Parameter identification errors at different SNR levels.

Parameter	Errors at 40 dB	Errors at 34 dB	Errors at 30 dB
R_s	0.61%	3.26%	7.29%
L_q	0.58%	0.25%	1.06%
J	9.09%	17.1%	28.1%
B_f	2.13%	9.81%	20.4%
τ_L	13.3%	34.3%	64.1%

D. ALTERNATIVE FLUX LINKAGE MODELING AND ONLINE IDENTIFICATION

As mentioned in Section I, there are alternative online identification techniques. To contrast the proposed method with existing ones, the approach in [24] also provides an empirical flux linkage model to replace look up tables that instead relies on a Fourier series function in the exponent of the model. Online data is used with the assumption that all the other electrical parameters are known such as $\psi_{s,\max}$ and R_s, and that an initial guess of the parameters is known *a priori* to improve the convergence of their iterative method. It is based on an earlier work [23] with more Fourier series terms, however, the earlier approach did not converge when attempted in the current simulation. Also, the alternative iterative method in [27] is more comprehensive as it furnishes all electric and mechanical parameters of the SRM, however, it relies on the assumption of linear magnetics, which does not represent SRMs operating at their rated conditions.

The flux linkage model [24] is given by

$$\psi_s = \psi_{s,\max}\left(1 - e^{-i_s f_s(\theta_q)}\right), \tag{36}$$

$$f_s(\theta_q) = a_0 + a_1\cos(\theta_q) + a_2\cos(2\theta_q) + a_3\cos(3\theta_q), \tag{37}$$

where $\theta_q = \theta + \pi/N_r$ as chosen in [24], i.e., it starts at the unaligned (quadrature) position. Rearranging the flux model in regressor form

$$Y = \phi^T \chi, \tag{38}$$

with,

$$Y \triangleq \ln\left(\frac{\psi_{s,max}}{\psi_{s,max} - \psi_s}\right), \tag{39}$$

$$\phi^T \triangleq \left[\, i_s \;\; i_s\cos(\theta_q) \;\; i_s\cos(2\theta_q) \;\; i_s\cos(3\theta_q) \,\right], \tag{40}$$

$$\chi^T \triangleq \left[\, a_0 \;\; a_1 \;\; a_2 \;\; a_3 \,\right], \tag{41}$$

where, ϕ and Y contain the measurable quantities, χ are the unknown parameters, and $\psi_s = \int v_s - i_s R_s dt$ is calculated online.

The following recursive least squares (RLS) discrete-time equations are calculated at time iteration k

$$P_k = \frac{1}{\gamma}\left[P_{k-1} - \frac{P_{k-1}\phi_k\phi_k^T P_{k-1}}{\gamma + \phi_k^T P_{k-1}\phi_k}\right], \tag{42}$$

$$\epsilon_k = Y_k - \phi_k^T \chi_{k-1}, \tag{43}$$

$$\chi_k = \chi_{k-1} + P_k\phi_k\epsilon_k. \tag{44}$$

This identification method was implemented in Simulink by adding the block shown in Fig. 9 and its RLS block in Fig. 10. Phase a parameters are estimated, with the RLS block enabled whenever phase a is active. Moreover, a discrete-time Butterworth second order low pass filter is applied to the signals with a cuttoff frequency $f_c = 1$ kHz.

The main issue observed with the method was that the parameters in χ converge to a new set of values with every phase a cycle. Specifically, there are four parameter sets that were heuristically identified from the resulting plots with the aid of the error function ϵ. After converging to a set of values that yield a low error, they diverge again before the end of each cycle as shown in Fig. 11 for the parameters and Fig. 12 for the error function ϵ. To achieve this temporary convergence, the following additional factors were considered:

1) Selecting the appropriate cutoff frequency f_c was necessary to avoid over filtering of the flux linkage signal if f_c is too low and to avoid divergence of χ if f_c is too high.
2) The RLS parameter γ has to be $0.95 < \gamma < 1.00$, so $\gamma = 0.97$ was selected.

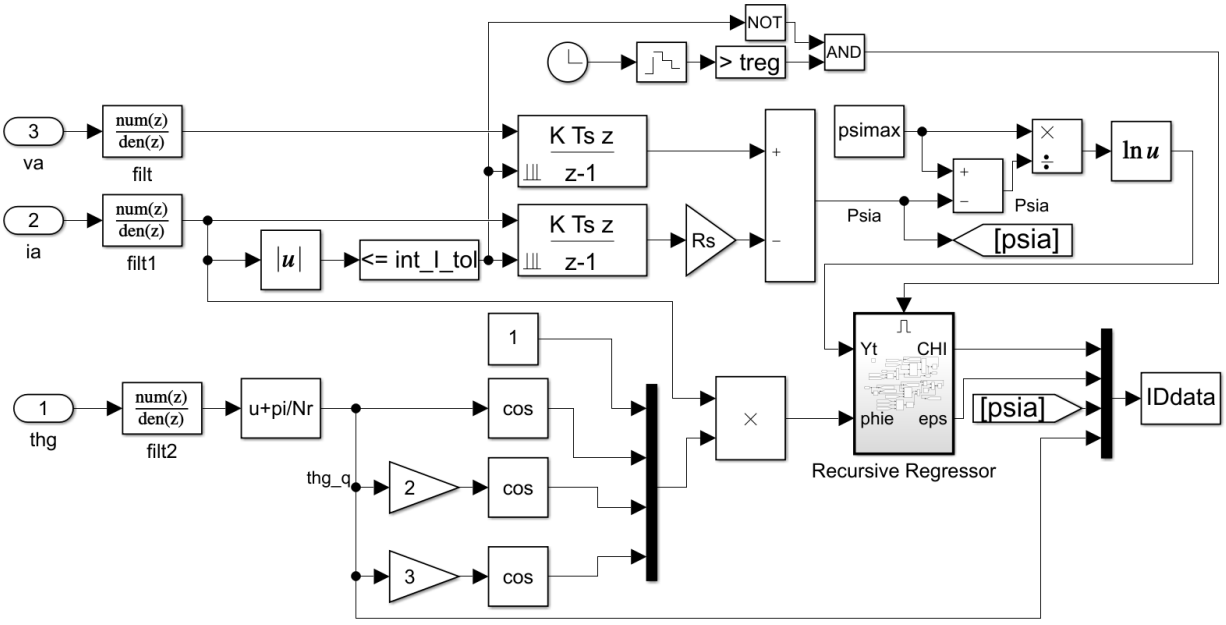

FIGURE 9. RLS Simulink online identification method.

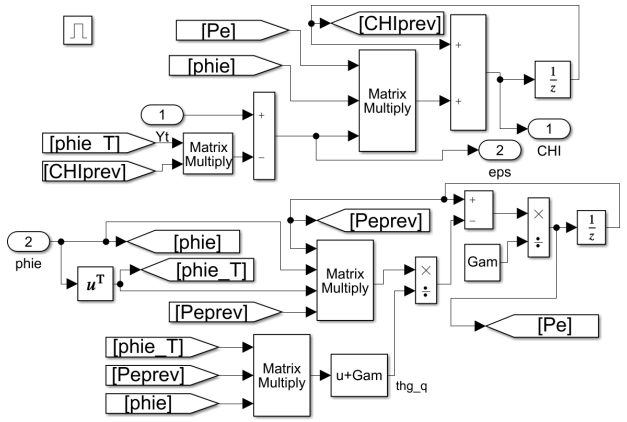

FIGURE 10. RLS regressor block.

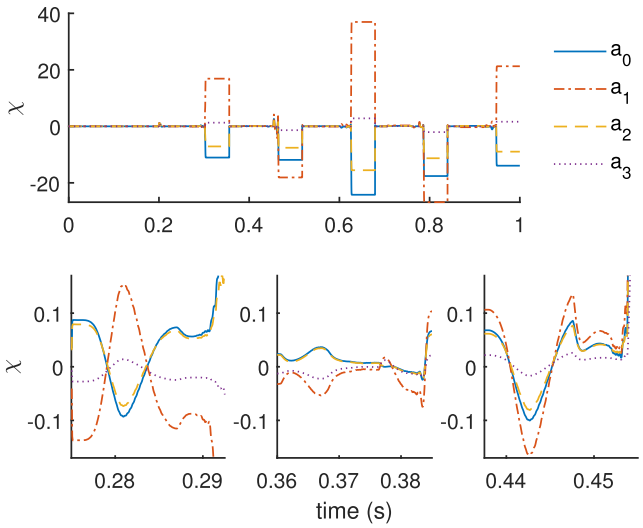

FIGURE 11. RLS identification of the four parameters in χ vs. time with zoomed subplots.

3) The controller was set to a fixed reference current at the rated value $I_{s,ref} = 180$ A for a 1 s interval.
4) The machine was slowed down by increasing the load's coefficient of viscous friction to $B_{f,L} = 2.2$ N.m.s to collect more data when phase a is enabled.
5) Identification starts at $t = 0.2$ s to skip over initial transients.

As a result, the four χ sets of identified parameters are shown in Table 4. These result in four alternative estimated waveforms for $\psi_{a,est}$ as shown in Fig. 13. Note that the y-axis in these figures is restricted for clarity and does not show the diverging waveforms. It can be seen that each one of the estimated $\psi_{a,est}$ waveforms closely matches the actual ψ_a albeit once every four cycles. In conclusion, the implementation of the RLS algorithm under these simulated conditions of the SRM is not reliable in producing a single empirical function that captures the behavior of the flux linkage ψ_a.

TABLE 4. Parameter χ sets for the RLS online identification method.

Parameter	Set 1	Set 2	Set 3	Set 4
a_0	−0.04140	0.073102	−0.0086311	0.085428
a_1	0.16256	−0.11470	−0.042687	0.13470
a_2	−0.041207	0.067293	−0.010092	0.076439
a_3	0.047421	−0.024550	−0.011878	0.025977

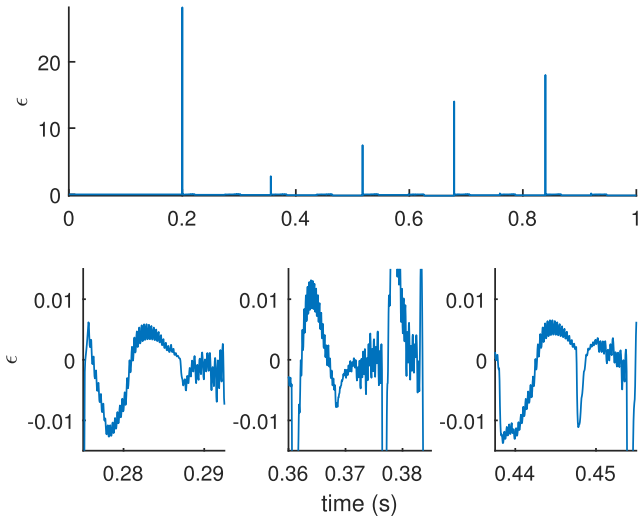

FIGURE 12. RLS error function ϵ vs. time with zoomed subplots.

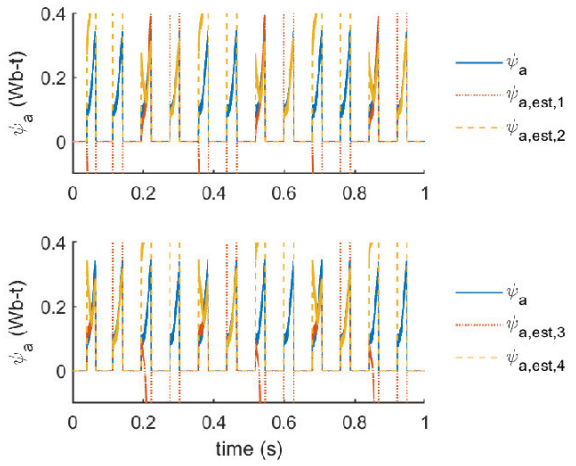

FIGURE 13. The actual and four RLS estimated flux linkage waveforms vs. time.

V. CONCLUSION

An online parameter identification method was developed in this work for the SRM, which uses a new nonlinear empirical model of the machine. All electrical and mechanical parameters of the model were identified without *a priori* knowledge or offline measurements. It was shown that 2 seconds of data collection time sufficiently excited the parameter identification regressor equations, with a computation time of 0.45 seconds to obtain all the parameters. Also, the resulting analytical model closely predicted the flux linkages and induced electromagnetic torque waveforms compared to their measured counterparts in simulation. In addition, the impact of disturbance due to noise in measurements was investigated. It was found that the electrical parameter identification was reliable, and that the mechanical parameter identification only deteriorated at an SNR of 30 dB and lower. Key features of the proposed method are the non-iterative algorithm that would otherwise require proof of convergence and the ability to identify each phase independently. For comparison, a recursive least squares method was demonstrated that diverged in the simulation. The proposed online method is therefore more comprehensive and more reliable than existing iterative methods. It is also particularly beneficial for embedded system drives that require a fast algorithm that enables periodic diagnostics of the machine, is capable of independently detecting anomalies in each phase, and can support advanced torque ripple minimization control techniques.

REFERENCES

[1] J. Stephan, M. Bodson, and J. Chiasson, "Real-time estimation of the parameters and fluxes of induction motors," *IEEE Trans. Ind. Appl.*, vol. 30, no. 3, pp. 746–759, May 1994.

[2] A. Oteafy, J. Chiasson, and M. Bodson, "Online identification of the rotor time constant of an induction machine," in *Proc. Amer. Control Conf.*, 2009, pp. 4373–4378.

[3] A. M. A. Oteafy, J. N. Chiasson, and S. Ahmed-Zaid, "Development and application of a standstill parameter identification technique for the synchronous generator," *Int. J. Electr. Power Energy Syst.*, vol. 81, pp. 222–231, Oct. 2016.

[4] A. M. A. Oteafy and J. N. Chiasson, "A standstill parameter identification technique for the divided winding rotor synchronous generator," in *Proc. IEEE Int. Conf. Power Energy (PECon)*, Dec. 2014, pp. 99–104.

[5] J. Chiasson, *Modeling and High Performance Control of Electric Machines*, vol. 26. Hoboken, NJ, USA: Wiley, 2005.

[6] S. S. Ramamurthy and J. C. Balda, "Sizing a switched reluctance motor for electric vehicles," *IEEE Trans. Ind. Appl.*, vol. 37, no. 5, pp. 1256–1264, Sep. 2001.

[7] M. Ilic-Spong, R. Marino, S. Peresada, and D. Taylor, "Feedback linearizing control of switched reluctance motors," *IEEE Trans. Autom. Control*, vol. AC-32, no. 5, pp. 371–379, May 1987.

[8] S. Mir, M. E. Elbuluk, and I. Husain, "Torque-ripple minimization in switched reluctance motors using adaptive fuzzy control," *IEEE Trans. Ind. Appl.*, vol. 35, no. 2, pp. 461–468, Mar. 1999.

[9] N. Inanc and V. Ozbulur, "Torque ripple minimization of a switched reluctance motor by using continuous sliding mode control technique," *Electr. Power Syst. Res.*, vol. 66, no. 3, pp. 241–251, Sep. 2003.

[10] M. Ilic-Spong, T. J. E. Miller, S. R. Macminn, and J. S. Thorp, "Instantaneous torque control of electric motor drives," *IEEE Trans. Power Electron.*, vol. PE-2, no. 1, pp. 55–61, Jan. 1987.

[11] V. Vujičić, "Minimization of torque ripple and copper losses in switched reluctance drive," *IEEE Trans. Power Electron.*, vol. 27, no. 1, pp. 388–399, Jan. 2012.

[12] I. Husain, "Minimization of torque ripple in SRM drives," *IEEE Trans. Ind. Electron.*, vol. 49, no. 1, pp. 28–39, Aug. 2002.

[13] X. Li and P. Shamsi, "Inductance surface learning for model predictive current control of switched reluctance motors," *IEEE Trans. Transport. Electrific.*, vol. 1, no. 3, pp. 287–297, Oct. 2015.

[14] V. K. Sharma, S. S. Murthy, and B. Singh, "An improved method for the determination of saturation characteristics of switched reluctance motors," *IEEE Trans. Instrum. Meas.*, vol. 48, no. 5, pp. 995–1000, Oct. 1999.

[15] A. D. Cheok and N. Ertugrul, "Computer-based automated test measurement system for determining magnetization characteristics of switched reluctance motors," *IEEE Trans. Instrum. Meas.*, vol. 50, no. 3, pp. 690–696, Jun. 2001.

[16] J. Lindsay, R. Arumugam, and R. Krishnan, "Finite-element analysis characterisation of a switched reluctance motor with multitooth per stator pole," *IEE Proc. B, Electr. Power Appl.*, vol. 133, no. 6, pp. 347–353, 1986.

[17] D. Ursu, V. Gradinaru, B. Fahimi, and I. Boldea, "Six-phase BLDC reluctance machines: FEM-based characterization and four-quadrant control," *IEEE Trans. Ind. Appl.*, vol. 51, no. 3, pp. 2105–2115, May 2015.

[18] H. Le-Huy and P. Brunelle, "A versatile nonlinear switched reluctance motor model in Simulink using realistic and analytical magnetization characteristics," in *Proc. 31st Annu. Conf. IEEE Ind. Electron. Soc. (IECON)*, Nov. 2005, p. 6.

[19] T. Miller and M. McGilp, "Nonlinear theory of the switched reluctance motor for rapid computer-aided design," *IEE Proc. B, Electr. Power Appl.*, vol. 137, no. 6, pp. 337–347, 1990.
[20] T. Miller, M. Glinka, M. McGilp, C. Cossar, G. Gallegos-Lopez, D. Ionel, and M. Olaru, "Ultra-fast model of the switched reluctance motor," in *Proc. 33rd IAS Annu. Meeting*, vol. 1, 1998, pp. 319–326.
[21] V. Vujičić and S. N. Vukosavic, "A simple nonlinear model of the switched reluctance motor," *IEEE Trans. Energy Convers.*, vol. 15, no. 4, pp. 395–400, Dec. 2000.
[22] A. Ferrero and A. Raciti, "A digital method for the determination of the magnetic characteristic of variable reluctance motors," *IEEE Trans. Instrum. Meas.*, vol. 39, no. 4, pp. 604–608, Aug. 1990.
[23] S. Mir, I. Husain, and M. E. Elbuluk, "Switched reluctance motor modeling with on-line parameter identification," *IEEE Trans. Ind. Appl.*, vol. 34, no. 4, pp. 776–783, Jul. 1998.
[24] M. Islam and I. Husain, "Self-tuning of sensorless switched reluctance motor drives with online parameter identification," in *Proc. 35th IAS Ann. Meeting World Conf. Ind. Appl. Electr. Energy*, vol. 3, 2000, pp. 1738–1744.
[25] J. F. Pan, N. C. Cheung, and Y. Zou, "High-precision control of LSRM based X–Y table for industrial applications," *ISA Trans.*, vol. 52, no. 1, pp. 105–114, Jan. 2013.
[26] S. Masoudi, M. R. Soltanpour, and H. Abdollahi, "Adaptive fuzzy control method for a linear switched reluctance motor," *IET Electr. Power Appl.*, vol. 12, no. 9, pp. 1328–1336, Nov. 2018.
[27] M. Aguado-Rojas, P. Maya-Ortiz, and G. Espinosa-Pérez, "On-line estimation of switched reluctance motor parameters," *Int. J. Adapt. Control Signal Process.*, vol. 32, no. 6, pp. 950–966, Jun. 2018.
[28] J. Gieras, *Electrical Machines: Fundamentals of Electromechanical Energy Conversion*. Boca Raton, FL, USA: CRC Press, 2016.
[29] Y. Chen, Y. Yao, and Y. Zhang, "A robust state estimation method based on SOCP for integrated electricity-heat system," *IEEE Trans. Smart Grid*, vol. 12, no. 1, pp. 810–820, Jan. 2021.
[30] Y. Chen, J. Ma, P. Zhang, F. Liu, and S. Mei, "Robust state estimator based on maximum exponential absolute value," *IEEE Trans. Smart Grid*, vol. 8, no. 4, pp. 1537–1544, Jul. 2017.
[31] Y. Chen, F. Liu, S. Mei, and J. Ma, "A robust WLAV state estimation using optimal transformations," *IEEE Trans. Power Syst.*, vol. 30, no. 4, pp. 2190–2191, Sep. 2014.

AHMED M. A. OTEAFY (Senior Member, IEEE) received the B.S. and M.S. degrees in electrical engineering from Kuwait University, in 2004 and 2006, respectively, and the Ph.D. degree in electrical and computer engineering from Boise State University, Boise, ID, USA, in 2011.

He is currently an Assistant Professor with Alfaisal University, Riyadh, Saudi Arabia, and the Director of the Joint Smart Grids and Electric Vehicles Research and Development Center (JSEC). He teaches power and control courses, such as renewable energy, power electronics, and modern control theory. His research interests include power systems, electric motors and generators, nonlinear control theory and applications, parameter identification and modeling, and stability analyses. His current focus is on microgrids research and development, and the development of a Boeing funded Solar Car Project.